Vehicular Collision Performance Evaluation of Concrete-Filled Steel Tubular Piers Designed According to Current Codes in the US, Europe, and China

Bo Hu[1] and Yu-Yang Liu[2]

Abstract: Current bridge codes in the US, Europe, and China specify vehicular collision loads for the design of piers. However, the performance of piers designed according to current codes in the three countries or regions is unknown yet. This paper presents a performance evaluation of concrete-filled steel tubular (CFST) piers subjected to vehicle collision. Before the evaluation, bridge specimens with a single CFST pier were designed in accordance with current bridge and structural codes in the three countries or regions, respectively. Then, a detailed finite-element (FE) model for simulating a truck collision with a CFST pier was developed and validated. By comparison with seven simplified FE models, the detailed FE model was further confirmed to be employed for the evaluation. In the evaluation, the effects of current codes in the three countries or regions, whether or not the vehicular collision load is considered, two pier heights (i.e., 6 and 12 m), two truck weights (i.e., 20 and 40 tons), and three impact speeds (i.e., 60, 100, and 140 km/h) on the performance of CFST piers were investigated. The evaluation results indicated that when a CFST pier in seismic zones is designed to resist vehicle collision according to current codes in the US and China, it only needs to meet the requirements of seismic design without additional consideration of the vehicular collision load. Moreover, a preliminary application condition should be added for the vehicular collision load specified by the current bridge code in Europe, that is, when the truck weight is more than 20 tons and/or the pier height is lower than 12 m. **DOI: 10.1061/(ASCE)BE.1943-5592.0001889**.

Author keywords: Concrete-filled steel tubular pier; Truck collision; Current design code; Performance evaluation; Detailed finite-element model.

Introduction

Piers are critical load-bearing members of bridge structures. During the service period, piers may suffer vehicle collision, such as the collision caused by a traffic accident or a terrorist attack. Vehicle collision with a pier may lead to damage to the pier or even collapse of a bridge structure that the pier belongs. Then, traffic will be interrupted, resulting in great economic loss and potential loss of life. Therefore, much attention has been paid to the performance of piers under vehicle collision (El-Tawil et al. 2005; Buth et al. 2010; Sharma et al. 2012, 2015; Abdelkarim and ElGawady 2017; Chen et al. 2017; Do et al. 2018; Fan et al. 2018; Auyeung et al. 2019; Cao et al. 2019a–c; Do et al. 2019; Hosseini et al. 2019; Saini and Shafei 2019; Chen et al. 2020; Li et al. 2020; Wu et al. 2020; Chen et al. 2021; Heng et al. 2021).

Concrete-filled steel tubular (CFST) piers, which have higher load carrying capacity and better ductility than traditional reinforced concrete (RC) piers, have been applied in bridge structures, such as the Severn railway bridge in the United Kingdom and the Labajin ditch bridge in China. Recently, the performance of CFST members under impact loading has attracted growing attention. Han et al. (2014) conducted a drop hammer impact test to compare the behavior of fixed–fixed and fixed–pinned supported CFST members subjected to transverse impact. Wang et al. (2013) experimentally investigated the effect of axial load levels on the response of CFST members under drop hammer lateral impact. These test results showed that CFST members present good performance under lateral impact loading. More recently, Saini and Shafei (2019) numerically simulated vehicles' impact on CFST and RC piers. They found that CFST piers primarily experience flexural deformation and failure, and the performance of CFST piers is significantly better than that of RC piers of the same sizes. Thus, it can be seen that CFST piers have great potential to resist vehicle collision. Nevertheless, so far, there are few studies on the behavior of CFST piers subjected to vehicle collision.

Actually, current bridge codes in many countries or regions have provisions for designing piers under vehicle collision. In the US, AASHTO LRFDBDS-9 (AASHTO 2020) suggests an equivalent static force of 2,700 kN at a distance of 1.5 m above ground as the vehicular collision load applied to piers. In Europe, BS EN 1992-2 (CEN 2005a) stipulates that the vehicular collision load is 1,000 kN in the direction of vehicle travel or 500 kN perpendicular to that direction, at a distance of 1.25 m above ground. In China, JTG D60-2015 (MOT 2015) specifies the same vehicular collision load as BS EN 1992-2 (CEN 2005a) but suggests a distance of 1.2 m above ground as the action position of the load. The vehicular collision load is only one kind of accidental action. As is known, the design of a pier needs to consider combinations of multiple actions, including permanent actions, variable actions, seismic actions, and accidental actions. Tables 1 and 2 list design values and combinations of actions specified by current bridge codes in the aforementioned three countries or regions, respectively. It can be seen that the current bridge code in each country or region has unique provisions. Moreover, for the design of CFST piers, current

[1]Associate Professor, College of Civil Engineering, Hefei Univ. of Technology, Hefei, Anhui 230009, China; Anhui Key Laboratory of Civil Engineering Structures and Materials, Hefei Univ. of Technology, Hefei, Anhui 230009, China (corresponding author). ORCID: https://orcid.org/0000-0001-6320-2425. Email: bohu@hfut.edu.cn

[2]College of Civil Engineering, Hefei Univ. of Technology, Hefei, Anhui 230009, China.

Note. This manuscript was submitted on October 12, 2021; approved on March 5, 2022; published online on April 12, 2022. Discussion period open until September 12, 2022; separate discussions must be submitted for individual papers. This paper is part of the ***Journal of Bridge Engineering***, © ASCE, ISSN 1084-0702.

Table 1. Design values of actions

Current bridge design code	Permanent actions Dead load	Seismic action	Variable actions: Vehicular live load	Variable actions: Braking load	Variable actions: Wind load	Accidental actions Vehicular collision load
AASHTO LRFDBDS-9 (AASHTO 2020)	Weight of all components of the structure, appurtenance, and utilities attached thereto	$F_{hs} = C_e M_t g$ $C_e = \begin{cases} C_{s,zero}C_{a,peak} + (C_{s,short}C_{a,0.2} - C_{s,zero}C_{a,peak})\frac{T}{0.2T_s} & 0 < T \le 0.2T_s \\ C_{s,short}C_{a,0.2} & 0.2T_s < T \le T_s \\ \frac{C_{s,long}C_{a,1.0}}{T} & T > T_s \end{cases}$	A combination of the truck or tandem and the lane load	25% of the axle weights of the truck or tandem, or 5% of the truck plus lane load or 5% of the tandem plus lane load	$F_w = 2.56 \times 10^{-6} V_d^2 K_z C_g C_D A_n$	1. Impact force: an equivalent static force of 2,700 kN acting in the direction of 0° to 15° with the edge of the pavement in a horizontal plane; 2. Height above ground: 1.5 m
BS EN 1992-2 (CEN 2005a)	Weight of all components of the structure, appurtenance, and utilities attached thereto	$F_{hs} = S_e M_t$ $S_e = \begin{cases} C_s\left[1 + (2.5C_d - 1)\frac{T}{T_B}\right]a_g & 0 \le T \le T_B \\ 2.5C_sC_da_g & T_B \le T \le T_C \\ 2.5C_sC_d\frac{T_C}{T}a_g & T_C \le T \le T_D \\ 2.5C_sC_d\frac{T_CT_D}{T^2}a_g & T_D \le T \le 4.0\text{s} \end{cases}$	Load Models 1, 2, and 3 should be taken into account	A fraction of the total maximum vertical loads corresponding to Load Model 1 is likely to be applied on Lane Number 1	$F_w = \frac{1}{2}\rho V_b^2 c_s c_d c_f c_e A_n$	1. Impact force: 1,000 kN in the direction of vehicle travel or 500 kN perpendicular to that direction; 2. Height above ground: 1.25 m
JTG D60-2015 (MOT 2015)	Weight of all components of the structure, appurtenance, and utilities attached thereto	$F_{hs} = S_e M_t$ $S_e = \begin{cases} 2.5C_iC_sC_d(6.0T + 0.4)a_{peak} & T < 0.1\text{s} \\ 2.5C_iC_sC_da_{peak} & 0.1\text{s} \le T \le T_g \\ 2.5C_iC_sC_d\frac{T_g}{T}a_{peak} & T_g < T \le 10.0\text{s} \end{cases}$	Lane load is used for the design of the structure and the vehicle load is used for the design of the structural element	10% of the lane load	$F_w = \frac{1}{2}\rho V_b^2 C_D A_n$	1. Impact force: 1,000 kN in the direction of vehicle travel or 500 kN perpendicular to that direction; 2. Height above ground: 1.2 m

Note: F_{hs} = horizontal seismic force; M_t = mass of an equivalent single-degree-of-freedom system; C_e = elastic seismic coefficient; g = acceleration of gravity; $C_{s,zero}$, $C_{s,short}$, and $C_{s,long}$ are the zero-, short-, and long-period site coefficients, respectively; $C_{a,0.2}$ and $C_{a,1.0}$ are the horizontal response spectral acceleration coefficients at 0.2- and 1.0-s period, respectively; $C_{a,peak}$ is peak ground acceleration coefficient; T = vibration period of a linear single-degree-of-freedom system; T_s = corner period at which spectrum changes from being independent of period to being inversely proportional to period; S_e = elastic response spectrum; a_g = design ground acceleration; T_B and T_C are the lower and upper limits of the period of the constant spectral acceleration branch, respectively; T_D = value defining the beginning of the constant displacement response range of the spectrum; C_s = site coefficient; C_d = damping correction coefficient; C_i = important coefficient; T_g = characteristic period of a linear single-degree-of-freedom system; F_w = wind force; V_d = design 3-s gust wind velocity; K_z = exposure and elevation coefficient; C_g = gust effect coefficient; C_D = drag coefficient; A_n = reference area of the structure or structural element; ρ = air density; V_b = basic wind velocity; and c_s, c_d, c_f, and c_e are the size, dynamic, force, and exposure coefficients, respectively.

Table 2. Combinations of actions

Current bridge design code		Limit states	Load factors: Permanent actions Dead load	Seismic action	Variable actions: Vehicular live load	Vehicular braking load	Wind load	Accidental actions Vehicular collision load
AASHTO LRFDBDS-9 (AASHTO 2020)		Strength I	γ_p	—	1.75	1.75	—	—
		Strength II	γ_p	—	1.35	1.35	—	—
		Strength III	γ_p	—	—	—	1.40	—
		Strength IV	γ_p	—	—	—	—	—
		Strength V	γ_p	—	1.35	1.35	0.40	—
		Extreme event I	γ_p	1.00	γ_{EQ}	γ_{EQ}	—	—
		Extreme event II	γ_p	—	0.50	0.50	—	1.00
		Service I	1.00	—	1.00	1.00	0.30	—
		Service II	1.00	—	1.30	1.30	—	—
		Service III	1.00	—	0.80	0.80	—	—
		Service IV	1.00	—	—	—	1.00	—
BS EN 1992-2 (CEN 2005a)	Ultimate	Persistent and transient	1.35	—	1.50	1.50	1.50	—
		Accidental	1.00	—	0.50	0.50	0.50	1.00
		Seismic	1.00	1.00	0.30	0.30	0.30	—
	Service	Characteristic	1.00	—	1.00	0.50	0.50	—
		Frequent	1.00	—	0.50	0.30	0.30	—
		Quasi-permanent	1.00	—	0.30	0.30	0.30	—
JTG D60-2015 (MOT 2015)		Strength	1.20	—	1.40	0.98	0.98	—
		Seismic	1.00	1.00	0.70	—	—	—
		Service	1.00	—	0.40	1.00	—	—
		Accidental	1.00	—	0.70	—	—	1.00

Note: γ_p = load factor for permanent actions; and γ_{EQ} = load factor for the live load applied simultaneously with the seismic load.

structural codes for CFST members need to be satisfied in addition to current bridge codes. In the US, Europe, and China, current structural codes, i.e., ANSI/AISC 360-10 (AISC 2010), BS EN 1994-2 (CEN 2005b), and GB 50936-2014 (MOHURD 2014), respectively, are also different in bearing capacity check and detailing requirements for CFST members, as listed in Table 3. This means that CFST piers designed according to the current bridge and structural codes in the US, Europe, and China may have different sectional dimensions, resulting in different vehicular collision performances. However, these differences are unknown yet.

In addition, full-scale tests of a vehicle collision with bridge piers are difficult to conduct because the cost of a collision test is extremely high. Therefore, numerical simulation has been an attractive alternative approach to studying the performance of piers under vehicle collision. When finite-element (FE) modeling the collision between a vehicle and a pier, two important issues need to be addressed. One is whether or not the boundary components of the pier need to be modeled, including the superstructure, cap beam, and substructure. The other is how to model the boundary components. In the FE models of Buth et al. (2010), Chen et al. (2017), and Cao et al. (2019a–c), each pier was assumed to be fixed both at the top and the bottom. They did not consider the effects of the boundary components on the impact response of bridge piers. Sharma et al. (2012, 2015) still fixed each pier at the bottom but added a mass body on the top to model the load from the superstructure. Nevertheless, the lateral confinement of the superstructure to the pier top, which is caused by the contact and friction between the superstructure and the cap beam, was neglected. Chen et al. (2020) and Li et al. (2020) employed solid elements to model the cap beam and substructure and then simplified the superstructure as uniform loads or a mass body on the top of the cap beam. Numerical analysis by Do et al. (2018) showed that compared with the detailed FE model, simplifications by Chen et al. (2020) and Li et al. (2020) for the superstructure only result in accurate predictions for the impact forces but not for the deformation of the pier. El-Tawil et al. (2005), Abdelkarim and ElGawady (2017), Fan et al. (2018), Do et al. (2018, 2019), Auyeung et al. (2019), and Saini and Shafei (2019) used solid or beam elements to model the superstructure, cap beam, and substructure. However, the solid and beam elements were assumed to be elastic. The influences of the real material properties of the boundary components were not considered. Especially for the cap beam and substructure, which are directly connected with the pier, the use of elastic material models should be more cautious. Hence, before numerically studying the performance of CFST piers under vehicle collision, it is necessary to develop a rational FE model.

Therefore, this paper aims to evaluate the performance of CFST piers subjected to vehicle collision. Before the evaluation, bridge specimens with a single CFST pier were designed in accordance with current bridge and structural codes in the US (AASHTO 2020; AISC 2010), Europe (CEN 2005a, b), and China (MOT 2015; MOHURD 2014), respectively. Then, a detailed FE model was developed, validated, and confirmed for simulating vehicle collision with a CFST pier in the evaluation. The evaluation results are expected to provide a comparative reference for the research and design of CFST piers subjected to a vehicle collision in the US, Europe, and China.

Design of Bridge Specimens with a Single CFST Pier

Current Bridge and Structural Design Codes in the US, Europe, and China

Bridge specimens were designed as highway bridges. Each bridge specimen had a single pier. The pier was designed as a CFST member, while the superstructure, cap beam, and substructure were

Table 3. Bearing capacity checks and detailing requirements for CFST members

Current structural design code	Bearing capacity check	Detailing requirement
ANSI/AISC 360-10 (AISC 2010)	For members in combined axial compression and flexure: $\frac{N}{\phi_c N_n}+\frac{8M}{9\phi_b M_n}\le 1$ for $\frac{N}{\phi_c N_n}\ge 0.2$; $\frac{N}{2\phi_c N_n}+\frac{M}{\phi_b M_n}\le 1$ for $\frac{N}{\phi_c N_n}<0.2$, $N_n=f_yA_s+0.95f_cA_c$, $M_n=M_p$ For members in shear: $V\le\phi_v V_n=\phi_v\left(0.6f_yA_s+20\lambda_m\sqrt{f_c}A_c/\pi\right)$	$\frac{A_s}{A_c}\ge 1\%$
BS EN 1994-2 (CEN 2005b)	For members in axial compression: $N\le\chi N_p$, $N_p=f_yA_s+f_{cd}A_c$ For members in flexure: $\eta M\le 0.9\mu M_p$ For members in shear: $V\le V_p=\frac{f_yA_s}{\sqrt{3}\gamma_m}+\frac{4}{\pi}\left(0.035k^{1.5}\sqrt{f_{ck}}+\frac{0.15N}{A_c}\right)A_c$	$0.2\le\frac{A_sf_y}{A_sf_y+A_cf_c}\le 0.9$
GB 50936-2014 (MOHURD 2014)	For members in combined axial compression, flexure, and shear: $\frac{N}{\varphi N_0}+\frac{\beta_m M}{1.5M_u(1-0.4N/N'_E)}+\left(\frac{V}{V_u}\right)^2\le 1$ for $\frac{N}{\varphi N_0}\ge 0.255\left[1-\left(\frac{V}{V_u}\right)^2\right]$; $-\frac{N}{2.17\varphi N_0}+\frac{\beta_m M}{M_u(1-0.4N/N'_E)}+\left(\frac{V}{V_u}\right)^2\le 1$ for $\frac{N}{\varphi N_0}<0.255\left[1-\left(\frac{V}{V_u}\right)^2\right]$ $N_0=f_{sc}(A_s+A_c)$, $M_u=\gamma_{pd}W_{sc}f_{sc}$, $V_u=0.71f_{sv}(A_s+A_c)$, $N'_E=\frac{\pi^2E_{sc}(A_s+A_c)}{1.1\lambda^2}$	$0.5\le\frac{A_sf_y}{A_cf_c}\le 2$

Note: N = axial compressive force; N_0 = nominal strength; M = bending moment; V = shear force; N_n, M_n, and V_n = nominal axial compressive, flexural, and shear strengths, respectively; ϕ_c, ϕ_b, and ϕ_v = resistance factors for compression, flexure, and shear, respectively; f_y = specified yield strength of the steel tube; f_c = specified compressive strength of concrete; A_s and A_c = cross-sectional areas of steel tubular and concrete sections, respectively; M_p = moment corresponding to plastic stress distribution over the composite cross section; λ_m = modification factor; N_p, M_p, and V_p = design values of the axial compressive, flexural, and shear resistances, respectively; f_{cd} and f_{ck} = design and characteristic values of the cylinder compressive strength of concrete, respectively; χ = reduction factor for flexural buckling; η = amplification factor for second-order effects; μ = factor related to design for compression and uniaxial bending; γ_m = partial factor for resistance of cross sections; k = size effect modification factor; N_0, M_u, and V_u = design values of the axial compressive, flexural, and shear strengths, respectively; β_m = equivalent moment coefficient; φ = stability coefficient; N'_E = critical buckling strength; λ = slenderness ratio; f_{sc} and f_{sv} = specified compressive and shear strengths of concrete filled steel tube, respectively; W_{sc} and E_{sc} = composite section and elastic moduli, respectively; and γ_{pd} = plastic development coefficient.

designed as RC members. Hence, current design codes for highway RC bridges, i.e., AASHTO LRFDBDS-9 (AASHTO 2020) in the US, BS EN 1992-2 (CEN 2005a) in Europe, and JTG D60-2015 (MOT 2015) in China, were selected. Meanwhile, current structural design codes for CFST members, i.e., ANSI/AISC 360-10 (AISC 2010) in the US, BS EN 1994-2 (CEN 2005b) in Europe, and GB 50936-2014 (MOHURD 2014) in China, were also employed.

The aforementioned three current bridge codes have similar design principles and procedures. However, there are differences in design values and combinations of actions among these codes, as listed in Tables 1 and 2, respectively. The actions include permanent actions, seismic actions, variable actions, and accidental actions. It should be noted that for accidental actions, only the vehicular collision load was considered herein. This is because one of the aims of this paper is to investigate the influence of the vehicular collision load on the performance of CFST piers under truck impact. Moreover, multiple accidental actions usually do not occur at the same time.

Concrete-filled steel tubular piers were designed as column members in axial compression, flexure, and shear. Consequently, Table 3 lists the bearing capacity checks of CFST members subjected to axial compression, flexure, and shear specified by the aforementioned three structural design codes. For CFST members, ANSI/AISC 360-10 (AISC 2010), BS EN 1994-2 (CEN 2005b), and GB 50936-2014 (MOHURD 2014) also suggest the minimum steel ratio, steel contribution ratio, and confinement coefficient to consider detailing requirements, respectively. The ranges of the values of these ratios are also listed in Table 3.

Design Flow

The main purpose of this paper is to evaluate the effect of the provisions of the current bridge and structural design codes in the three countries or regions on the vehicular collision performance of CFST piers. Therefore, for each bridge specimen, the CFST pier was designed according to the current bridge and structural codes in the same country or region (i.e., the US, Europe, or China). On the other hand, in order to eliminate the influences of boundary components, the superstructure, cap beam, and substructure were designed only in accordance with the current bridge code in China. Meanwhile, the design of boundary components met the requirements of current bridge codes in the US and Europe. The design flow of a bridge specimen is shown in Fig. 1.

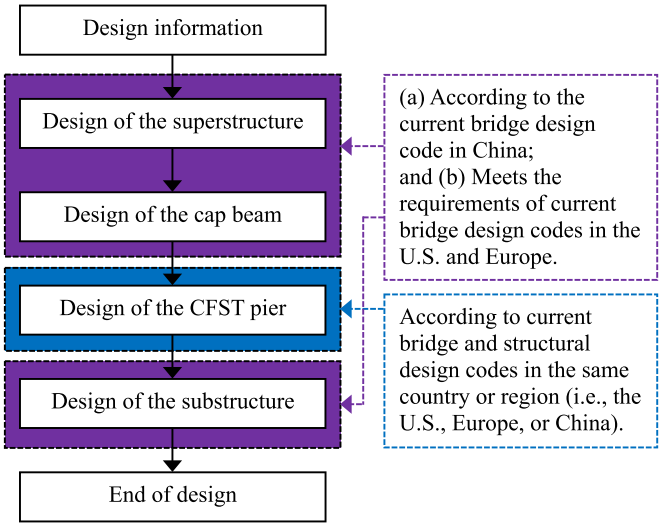

Fig. 1. Design flow of a bridge specimen.

All the bridge specimens were designed using the same design information. The design information appeared in China and included the following: (1) the grade of the highway was Grade I; (2) the seismic fortification category was Class B; (3) the seismic fortification intensity was 7°; (4) the site category was Class I; and (5) the terrain category was Class C.

Design of the Superstructure, Cap Beam, and Substructure

According to JTG D60-2015 (MOT 2015), the superstructure, cap beam, and substructure were designed, and the corresponding structural drawings are presented in Fig. 2. The superstructure included two bridge girders with a span of 20 m. Each bridge girder comprised four side-by-side T-section girders. All the T-section girders had a width of 2,200 mm and a height of 1,500 mm. The superstructure transmitted the gravity load to the pier through elastomeric bearing pads with polytetrafluroethylene (PTFE) sliding surfaces. Each girder was assumed to rest on two bearing pads. All the bearing pads had sectional dimensions of 200 × 200 mm, a total thickness of 37 mm, and a shear modulus of 0.608 MPa. The cap beam was 8,000 mm in width, 1,100 mm in height, and 1,400–1,700 mm in depth. The substructure had a length of 4,000 mm, a width of 4,000 mm, and a height of 3,000 mm. The superstructure, cap beam, and substructure were RC members. Steel bars and concrete had the strength grades of HRB400 and C50, respectively.

Design of CFST Piers

For each CFST pier, two annular plates were welded at the top and the bottom of the steel tube, respectively. The top annular plate was used to improve the connection behavior between the CFST pier and the cap beam. It was designed in accordance with the

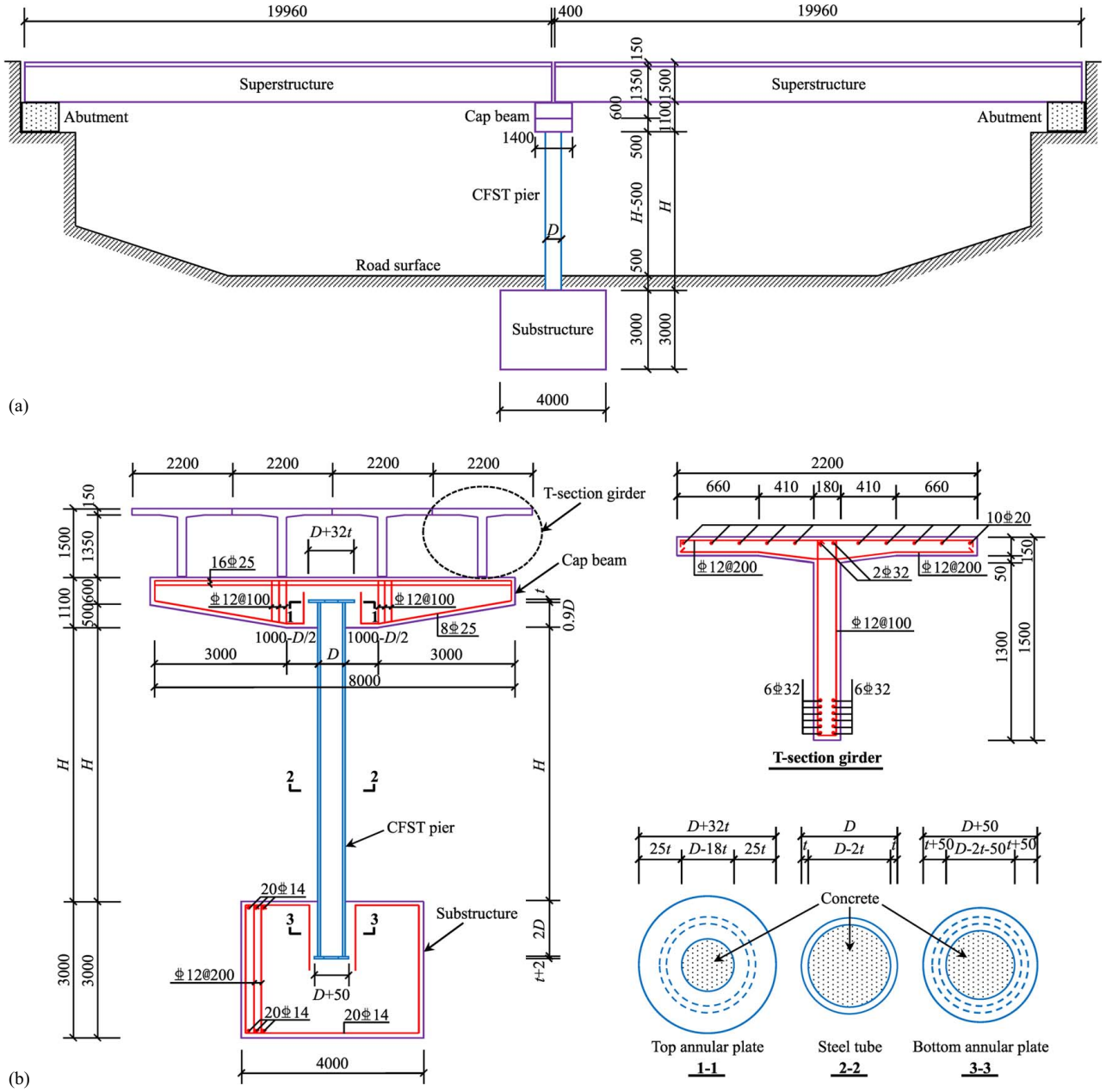

Fig. 2. Structural drawings of a bridge specimen (in mm): (a) elevation view; and (b) cross sections.

suggestion of Stephens et al. (2016). The bottom annular plate was utilized to prevent the CFST pier from being pulled out of the substructure. Its design was based on the inserted column footing specified by GJBT-919 (MOC 2006). The construction details of the top and bottom annular plates can be seen in Fig. 2(b). The strength grades of the steel tube and annular plates were Q345. The core concrete had a strength grade of C50.

Table 4 lists the sectional dimensions of CFST piers of all the bridge specimens after the design. It should be noted that all the sectional dimensions are the minimum values that meet the requirements of current design codes. A total of 12 CFST piers were designed. These CFST piers were divided into three groups according to the country or region where the current bridge and structural design codes are issued. Each group included four CFST piers. The influence parameters contained whether or not the vehicular collision load is considered and two pier heights (i.e., 6 and 12 m).

It is clear from Table 4 that CFST piers designed according to current codes in the US (AASHTO 2020; AISC 2010) are of the greatest sectional dimensions regardless of whether the vehicle collision load is considered. This indicates that the design of CFST piers carried out according to current codes in the US (AASHTO 2020; AISC 2010) is more conservative. Compared with ignoring the vehicular collision load, the sectional dimensions of CFST piers become larger when considering the vehicle collision load. This implies that the vehicle collision loads specified by current bridge codes in the US (AASHTO 2020), Europe (CEN 2005a), and China (MOT 2015) affect the design of CFST piers. When the pier height increases from 6 to 12 m, the sectional dimensions of CFST piers also become bigger. This is due to that the demand for sectional stiffness increases with an increase in pier height.

Table 4. Design and numerical results of CFST piers under vehicle collision

Current design codes				CFST pier			Performance level					
							20-ton truck			40-ton truck		
Country or region	Current bridge design code	Current structural design code	Is vehicular collision load considered?	Height (m)	Diameter (mm)	Thickness of the steel tube (mm)	60 km/h	100 km/h	140 km/h	60 km/h	100 km/h	140 km/h
US	AASHTO LRFDBDS-9 (AASHTO 2020)	ANSI/AISC 360-10 (AISC 2010)	Yes	6	1,000	17	OP	IO	IO	OP	IO	LS
			No	6	800	14	OP	IO	IO	IO	IO	LS
			Yes	12	1,000	19	OP	IO	IO	OP	IO	IO
			No	12	900	14	OP	IO	IO	OP	IO	IO
Europe	BS EN 1992-2 (CEN 2005a)	BS EN 1994-2 (CEN 2005b)	Yes	6	800	12	OP	IO	IO	IO	IO	LS
			No	6	600	12	IO	IO	LS	IO	LS	CP
			Yes	12	900	14	OP	IO	IO	OP	IO	IO
			No	12	750	14	OP	IO	IO	IO	IO	LS
China	JTG D60-2015 (MOT 2015)	GB 50936-2014 (MOHURD 2014)	Yes	6	700	12	OP	IO	LS	IO	LS	LS
			No	6	600	12	IO	IO	LS	IO	LS	CP
			Yes	12	800	14	OP	IO	IO	OP	IO	LS
			No	12	800	10	OP	IO	IO	OP	IO	LS

Detailed FE Model Development

Based on the geometric dimensions and material properties of bridge specimens designed previously, a detailed FE model was developed using LS-DYNA (LSTC 2020) to simulate vehicle collision with a CFST pier, as shown in Fig. 3. During the model development, the CFST pier FE model was validated by existing drop hammer impact tests (Han et al. 2014; Wang et al. 2013). The FE models of boundary components, including the superstructure, cap beam, and substructure, were confirmed by comparing the detailed FE model with seven simplified FE models.

FE Modeling

CFST Pier

A CFST pier is composed of a steel tube, top and bottom annular plates, and core concrete. For the steel tube, top and bottom annular plates, and core concrete, eight-node hexahedral constant stress solid elements were utilized to model them. The material models and properties for the steel tube, top and bottom annular plates, and core concrete were set as listed in Table 5. For the steel tube and annular plates, strain rate effects were considered using the Cowper and Symonds model (*LS-DYNA*, LSTC 2020) and the dynamic increase factor (DIF) of the yield strength of steel, DIF_y, was defined as follows:

$$\mathrm{DIF}_y = \frac{f_{y,d}}{f_{y,s}} = 1 + \left(\frac{\dot{\varepsilon}}{C}\right)^{1/p} \tag{1}$$

where $\dot{\varepsilon}$ = strain rate; $f_{y,s}$ and $f_{y,d}$ = static and dynamic yield strengths of steel, respectively; and C and p = strain rate parameters and were taken as 40 s^{-1} and 5, respectively.

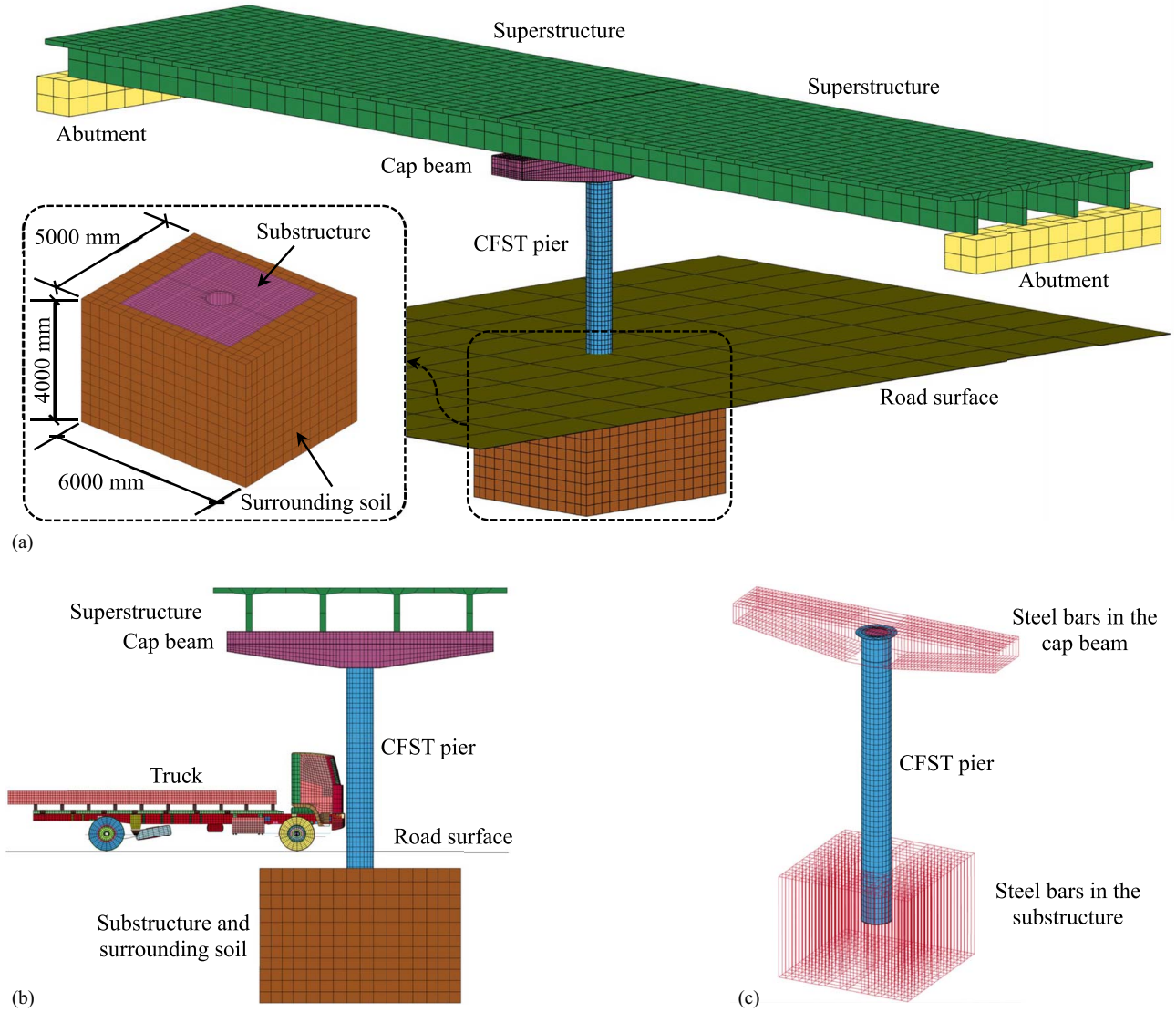

Fig. 3. Detailed FE model: (a) bridge specimen (oblique view); (b) modified truck model collision with CFST pier (side view); and (c) CFST pier and steel bars in the cap beam and substructure.

Table 5. Material models and properties in the detailed FE model

Component	Material model	Material properties					
		Density (kg/m^3)	Elastic modulus (GPa)	Poisson's ratio	Shear modulus (MPa)	Static yield strength (MPa)	Static compressive strength (MPa)
CFST pier							
Steel tube Annular plates	*MAT_PIECEWISE_LINEAR_PLASTICITY	7,800	200	—	—	345	—
Core concrete	*MAT_CONCRETE_DAMAGE_REL3	2,400	—	0.16	—	—	39.5[a]
Superstructure	*MAT_ELASTIC	2,550	34.5	—	—	—	—
Cap beam and substructure							
Steel bars	*MAT_PIECEWISE_LINEAR_PLASTICITY	7,800	200	—	—	400	—
Concrete	*MAT_CONCRETE_DAMAGE_REL3	2,400	—	0.16	—	—	39.5[a]
Surrounding soil	*MAT_SOIL_AND_FOAM	1,760	—	—	34.4	—	—
Abutment	*MAT_RIGID	—	—	—	—	—	—
Road surface	*MAT_RIGID	—	—	—	—	—	—

Source: Data from fib (2013).
[a]The value of 39.5 MPa was obtained by 0.79 × 50 MPa for C50 grade concrete.

Table 6. Contact algorithms in the detailed FE model

Interactions				
Master segment	Slave segment	Contact algorithm	Static coefficient of friction	Dynamic coefficient of friction
Steel tube	Top annular plate Bottom annular plate	*CONTACT_TIED_SURFACE_TO_SURFACE[a]	—	—
Steel tube Top annular plate Bottom annular plate	Core concrete	*CONTACT_AUTOMATIC_SURFACE_TO_SURFACE[b]	0.6	0.3
Superstructure	Cap beam Abutment	*CONTACT_AUTOMATIC_SURFACE_TO_SURFACE[b]	0.02	0.02
CFST pier	Cap beam Substructure	*CONTACT_AUTOMATIC_SURFACE_TO_SURFACE[b]	0.6	0.3
Substructure	Surrounding soil	*CONTACT_AUTOMATIC_SURFACE_TO_SURFACE[b]	0.6	0.3
Truck	CFST pier	*CONTACT_AUTOMATIC_SURFACE_TO_SURFACE[b]	0.3	0.2
Truck tiers	Road surface	*CONTACT_NODES_TO_SURFACE[c]	0.3	0.2
Truck		*CONTACT_AUTOMATIC_SINGLE_SURFACE[d]	0.4	0.3

[a]This contact algorithm is constraint-based.
[b]This contact algorithm is penalty-based and checks the penetration from slave nodes to master segments and from master nodes to slave segments.
[c]This contact algorithm is penalty-based and only checks the penetration from slave nodes to master segments.
[d]This contact algorithm is penalty-based and is used when master and slave segments are the same.

For core concrete, the model proposed in fib Model Code 2010 (fib 2013) was utilized to account for strain rate effects. Thus, the compressive and tensile strength DIFs of concrete, DIF_c and DIF_t, respectively, were determined by

$$\mathrm{DIF}_c = \frac{f_{c,d}}{f_{c,s}} = \begin{cases} \left(\frac{\dot{\varepsilon}}{30\times10^{-6}}\right)^{0.014} & \text{for } \dot{\varepsilon} \le 30\ \mathrm{s}^{-1} \\ 0.012\left(\frac{\dot{\varepsilon}}{30\times10^{-6}}\right)^{1/3} & \text{for } \dot{\varepsilon} > 30\ \mathrm{s}^{-1} \end{cases} \quad (2)$$

$$\mathrm{DIF}_t = \frac{f_{t,d}}{f_{t,s}} = \begin{cases} \left(\frac{\dot{\varepsilon}}{1\times10^{-6}}\right)^{0.018} & \text{for } \dot{\varepsilon} \le 10\ s^{-1} \\ 0.0062\left(\frac{\dot{\varepsilon}}{1\times10^{-6}}\right)^{1/3} & \text{for } \dot{\varepsilon} > 10\ s^{-1} \end{cases} \quad (3)$$

where $f_{c,s}$ and $f_{c,d}$ = static and dynamic compressive strengths of concrete, respectively; and $f_{t,s}$ and $f_{t,d}$ = static and dynamic tensile strengths of concrete, respectively.

For the interactions between the steel tube and annular plates, between the steel tube and core concrete, and between annular plates and core concrete, corresponding contact algorithms were selected to model them, as listed in Table 6.

Boundary Components

Boundary components of a CFST pier include the superstructure, cap beam, and substructure. These three consist of steel bars and concrete, as shown in Fig. 2(b). The cap beam and substructure are directly connected with the CFST pier. Thus, they were modeled using elastic–plastic material models to obtain more accurate dynamic responses of the CFST pier. During a vehicle collision with a CFST pier, the deformation of the superstructure does not affect the performance of the CFST pier because there is no direct contact between the superstructure and the pier. Moreover, numerical results of El-Tawil et al. (2005) indicated that the influence of the bearing pads is insignificant on the responses of a pier subjected to vehicle impact. Hence, it was assumed that the superstructure was of elastic material and directly rested on the tops of the cap beam and abutments. The material models and properties for the superstructure, cap beam, and substructure can be seen in Table 5. For the superstructure and the concrete in the cap beam and substructure, eight-node hexahedral constant stress solid elements were selected to model them. For modeling the steel bars in the cap beam and substructure, two-node Hughes–Liu beam elements were employed, as shown in Fig. 3(c). Strain rate effects of steel and concrete were also taken into account according to Eqs. (1)–(3), respectively. A perfect bond was assumed between steel bars and concrete.

Besides, the two abutments, which are used to support the substructure, were assumed to be rigid and fixed. A 6,000 × 5,000 × 4,000 mm surrounding soil was modeled to support the substructure, as shown in Fig. 3(a). The boundary surfaces of the surrounding soil, except for the upper surface were assumed to be fixed. A road surface with a thickness of 10 mm was modeled to support the moving vehicle, as shown in Figs. 3(a and b). It was assumed that the road surface was rigid and fixed. The abutments, surrounding soil, and road surface were modeled using eight-node hexahedral constant stress solid elements. The material models and properties for them are also presented in Table 5.

Vehicle

Buth et al. (2010) conducted an accident analysis of vehicle collisions with bridge piers. They found that most of the vehicles that hit the piers seriously were heavy trucks, e.g., 29.5- and 36.3-ton trucks. Hence, a European Standard EN-1317 test truck FE model with an initial weight of 16 tons developed by the National Crash Analysis Center (NCAC) (2011) was first downloaded. Then, the weight of the truck FE model was increased to 20 and 40 tons by modifying the weight of the engine and lumped masses. Note that the proportion of the weight of the engine and lumped masses were kept unchanged in the modification. The modified truck FE model is shown in Fig. 3(b).

Contact Algorithms, Hourglass Control, and Gravity Load Application

During a truck collision with a CFST pier, the interactions among the CFST pier, boundary components, and the truck should be treated carefully. Table 6 lists the contact algorithms used for the interactions, as well as static and dynamic coefficients of friction. Note that the sliding friction value of 0.02 for elastomeric bearing pads with PTFE sliding surfaces suggested by JTG/T 2231-01-2020 (MOT 2020) was used for the interactions between

the superstructure and the cap beam and between the superstructure and abutments.

For constant-stress solid elements used in the model, the single-point integration rule was employed, which implies the potential hourglass. Hence, the Flanagan–Belytschko stiffness form with exact volume integration was selected for controlling the hourglass, and the hourglass coefficient was set to be 0.05.

In addition, gravity loads caused by the CFST pier, boundary components, and the truck were applied using the *LOAD_BODY_Z keyword and kept unchanged during the collision.

Validation of the CFST Pier FE Model

Test results of CFST members under drop hammer impact conducted by Han et al. (2014) and Wang et al. (2013) were employed to validate the developed CFST pier FE model. A total of eight CFST members were simulated, as listed in Table 7. The modeling method described previously was utilized in this simulation. Material properties of steel and concrete provided in Han et al. (2014) and Wang et al. (2013) were used to define the corresponding material models. The eight CFST members had three end boundary conditions, including fixed–fixed, fixed–pinned, and fixed–sliding supports. For the fixed end, all translational and rotational degrees of freedom of the nodes on the surface were constrained, as shown in Figs. 4(b) and 5(b). When simulating the pinned support, a rigid cylinder was modeled to support the free end and all translational and rotational degrees of freedom of the nodes of the rigid cylinder were constrained, as shown in Fig. 4(b). For the interaction between the rigid cylinder and the CFST member, the *CONTACT_AUTOMATIC_SURFACE_TO_SURFACE contact algorithm was used and static and dynamic coefficients of friction were taken as 0.3 and 0.2, respectively. For the sliding end, translational degrees of freedom in all directions except for the axial direction of the nodes on the surface were constrained, as shown in Fig. 5(b). Additionally, for DZF31, an axial compressive load was applied on the rigid top of the sliding end and kept unchanged using the *LOAD_RIGID_BODY keyword. The axial compressive load was taken as the value provided in the test (Wang et al. 2013). The drop hammers were modeled using the *MAT_RIGID material model. For the interaction between the drop hammer and the CFST member, the same contact algorithm as that for the interaction between the truck and the CFST pier was adopted.

Figs. 6 and 7 compare the impact force and lateral deflection at the midspan time histories between FE analyses and tests, respectively. It is clear that impact force and lateral deflection versus time curves obtained by FE simulations are in good agreement with experimental results. Table 7 also presents the maximum impact forces and residual lateral deflections at the midspan of FE analyses and tests. The ratios of FE maximum impact forces to test ones have a mean value of 0.913 and a coefficient of variation (COV) of 0.130, while the ratios of FE residual lateral deflections at the midspan to test ones have a mean value of 1.078 and a COV of 0.078. It implies that the predictions by FE simulations agree well with experimental results. Moreover, Fig. 8 plots the comparisons of failure modes between FE analyses and tests. It can be seen that FE simulations accurately capture plastic deformation of the CFST members and even fracture of the steel tubes in tests. Therefore, the developed CFST pier FE model simulates the lateral impact performance of CFST members well and can be utilized for FE simulations of vehicle collisions.

Confirmation of Boundary Component FE Models

The detailed FE model can present more accurate results, but its computational cost is higher. Hence, seven simplified FE models,

Table 7. Comparisons between numerical and experimental results

Source	No.	Drop hammer		CFST member				Maximum impact force (kN)			Residual lateral deflection at the midspan (mm)		
		Mass (kg)	Speed (m/s)	Length (mm)	Diameter (mm)	Thickness of steel tube (mm)	Axial load level	Boundary condition	Test	FE	FE/Test	Test	FE	FE/Test
Han et al. (2014)	CC1	465.0	9.21	1,940	180	3.65	0.0	Fixed–fixed	800	621	0.776	64.0	68.2	1.066
	CC2	920.0	6.40	1,940	180	3.65	0.0	Fixed–fixed	627	520	0.829	70.0	68.1	0.973
	CS2	920.0	6.48	2,400	180	3.65	0.0	Fixed–pinned	595	548	0.921	103.0	103.2	1.002
	CS3	465.0	7.97	2,400	180	3.65	0.0	Fixed–pinned	710	729	1.027	78.0	81.3	1.042
Wang et al. (2013)	DZF22	229.8	7.60	1,200	114	3.50	0.0	Fixed–sliding	310	262	0.845	39.4	42.5	1.079
	DZF25	229.8	10.80	1,200	114	3.50	0.0	Fixed–sliding	380	340	0.895	72.4	84.9	1.173
	DZF26	229.8	11.70	1,200	114	3.50	0.0	Fixed–sliding	400	348	0.870	87.2	107.0	1.227
	DZF31	229.8	11.70	1,200	114	3.50	0.3	Fixed–sliding	320	366	1.144	101.7	108.0	1.062
Mean											0.913			1.078
COV											0.130			0.078

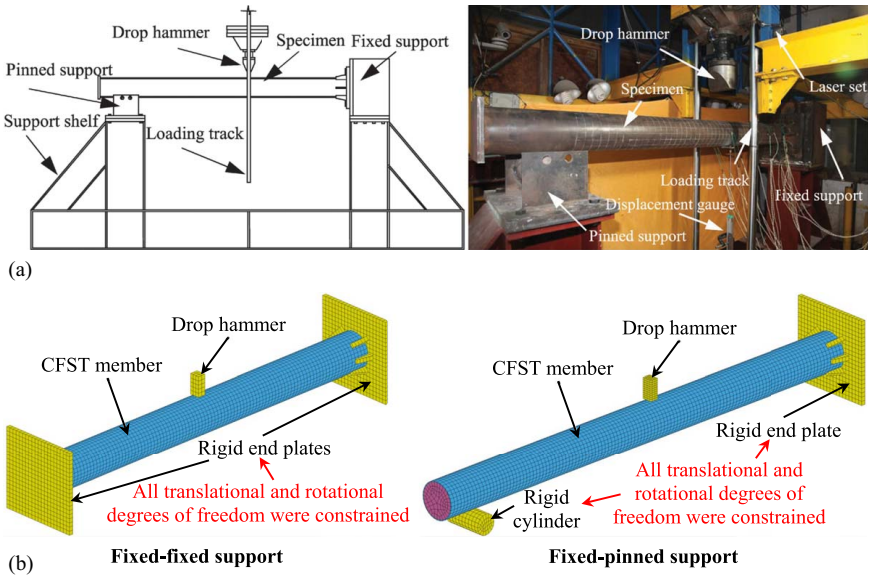

Fig. 4. Test setup and corresponding FE models: (a) test setup [reprinted from *Journal of Constructional Steel Research*, Vol. 92, L. Han, C. Hou, X. Zhao, K. Rasmussen, "Behaviour of high-strength concrete filled steel tubes under transverse impact loading," pp. 25–39, © 2014, with permission from Elsevier]; and (b) FE models.

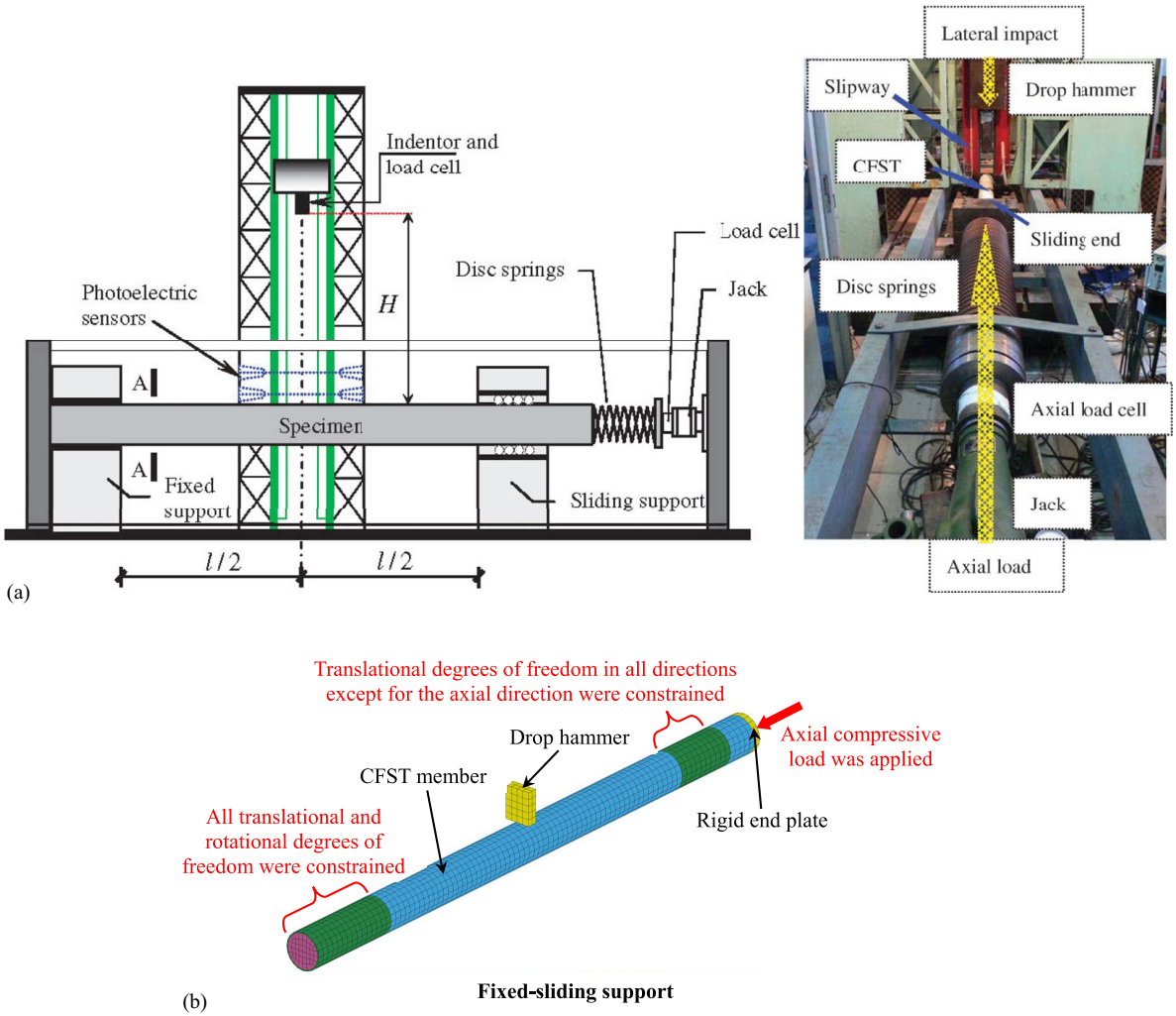

Fig. 5. Test setup and corresponding FE model: (a) test setup [reprinted from *Journal of Constructional Steel Research*, Vol. 80, R. Wang, L. Han, and C. Hou, "Behavior of concrete filled steel tubular (CFST) members under lateral impact: Experiment and FEA model," pp. 188–201, © 2013, with permission from Elsevier]; and (b) FE model.

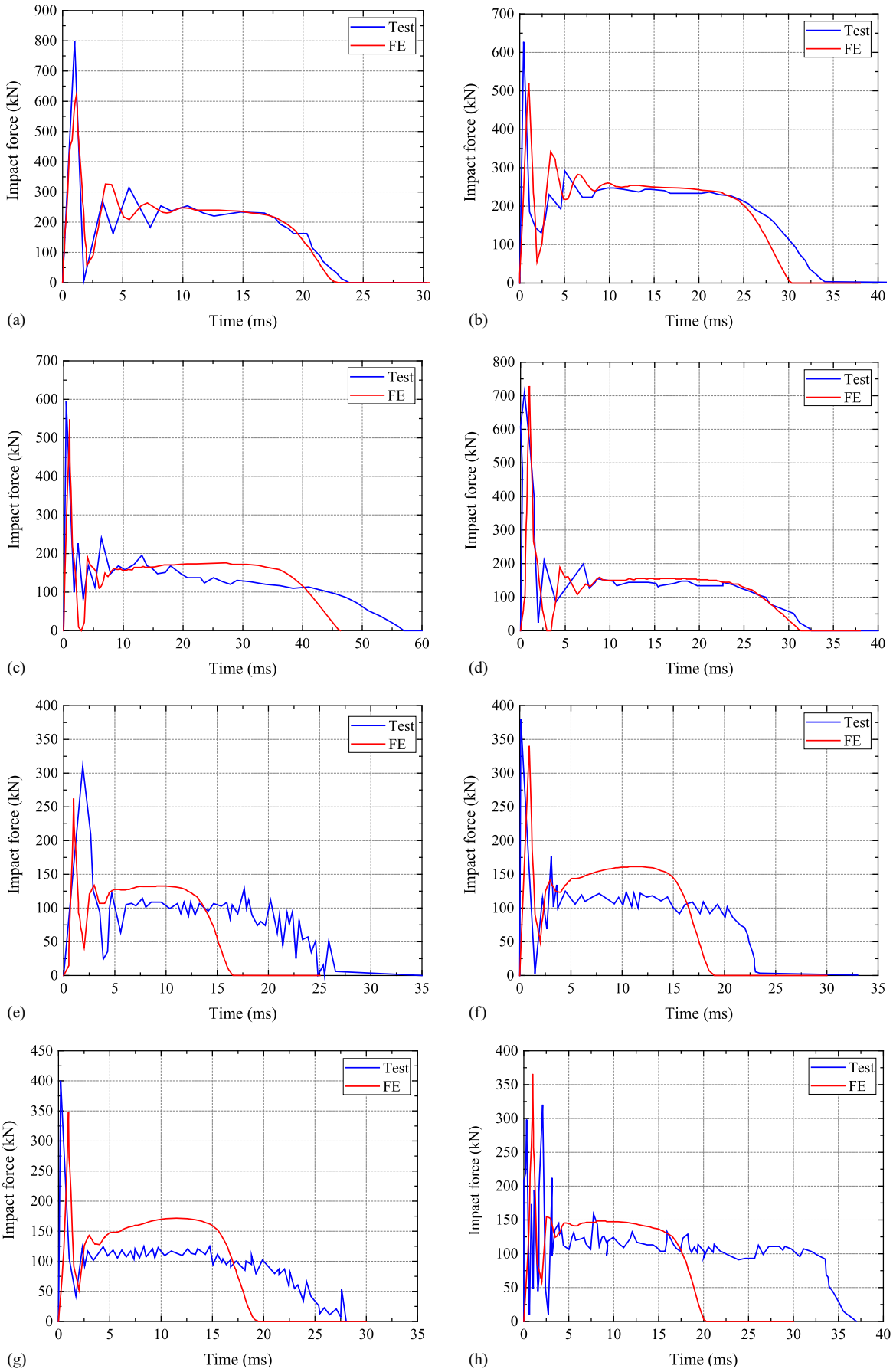

Fig. 6. Comparisons of impact force versus time curves: (a) CC1; (b) CC2; (c) CS2; (d) CS3; (e) DZF22; (f) DZF25; (g) DZF26; and (h) DZF31.

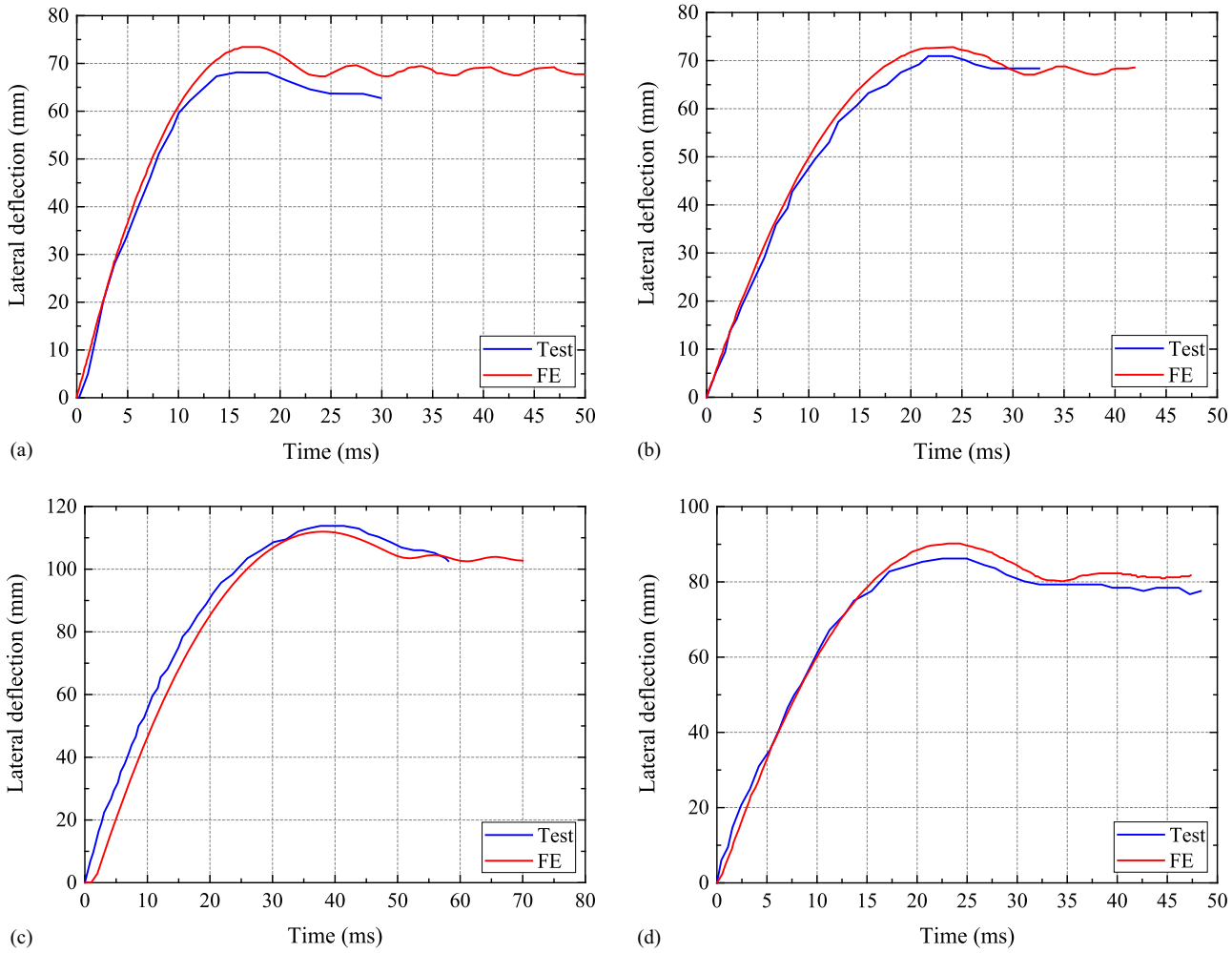

Fig. 7. Comparisons of lateral deflection at the midspan versus time curves: (a) CC1; (b) CC2; (c) CS2; and (d) CS3.

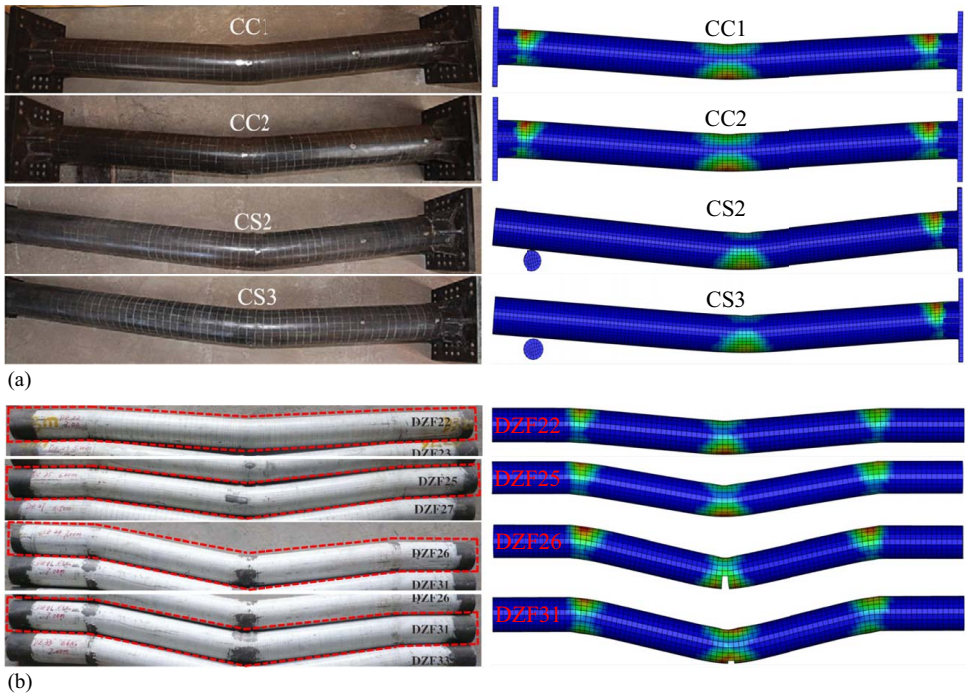

Fig. 8. Comparisons of failure modes: (a) comparisons with Han et al. (2014); and (b) comparisons with Wang et al. (2013).

which simplified the boundary components with varying degrees to save computational time, were employed to consider the possibility of replacing the detailed FE model, as shown in Fig. 9. The differences between the simplified and detailed FE models have been marked in different colors. In simplified FE Model I, the cap beam was modeled using the *MAT_ELASTIC material model. In simplified FE Model II, the substructure was modeled using the *MAT_ELASTIC material model. Simplified FE model III has been reported in Do et al. (2018), Fan et al. (2018), and Do et al. (2019), in which both the cap beam and the substructure were modeled using the *MAT_ELASTIC material models. In simplified FE Model IV, the top and bottom of the pier were fixed, which can also be seen in Buth et al. (2010), Chen et al. (2017), and Cao et al. (2019a–c). Simplified FE Model V is similar to the FE models in Sharma et al. (2012, 2015), in which the bottom of the pier was fixed and a rigid mass body was added on the top of the pier to simulate the gravity load imposed by the superstructure. In addition, the rigid mass body was only allowed to move vertically. In simplified FE Model VI, the superstructure was simplified as a rigid mass body on the top of the cap beam, which was also used in Li et al. (2020). Simplified FE Model VII is a further simplified version of simplified FE Model III, in which both the cap beam and the substructure were modeled using the *MAT_ELASTIC material models.

In order to compare the FE results of the detailed and simplified FE models, the CFST pier with a height of 6 m, a diameter of 800 mm, and a thickness of steel tube of 14 mm subjected to the 40-ton truck collision at an impact speed of 140 km/h was employed for the simulations. Figs. 10(a–c) depict the comparisons of impact force, lateral deflection at the midheight, and lateral deflection at the top time histories between the detailed and simplified FE models, respectively.

It is found from Fig. 10 that simplified FE Model I presents similar impact force and lateral deflection at the top-time curves with simplified FE Model III. It means that the material model used for the substructure has little effect on the dynamic response of the CFST pier under a truck collision when the cap beam is of elastic material. However, simplified FE Models I and III bring about greater second peak impact forces, lower residual lateral deflections at the midheight, and higher residual lateral deflections at the top than the detailed FE model. It might be attributed to the elastic material model used for the cap beam. When the material model used for the substructure changes from the elastic–plastic one to the elastic one, the second peak impact force increases and the residual lateral deflections at the midheight and the top decrease by comparing the detailed FE model with simplified FE Model II. It indicates that the influence of the material model used for the substructure on the performance of the CFST pier under truck impact is significant. Because the lateral displacements of the tops of the piers are constrained, simplified FE Models IV and V have no lateral displacement. Moreover, simplified FE Models IV and V result in greater second peak impact forces and smaller residual lateral deflections at the midheight than the detailed FE model. It demonstrates that the effects of boundary components cannot be ignored. When the superstructure was modeled using the rigid mass body instead of the solid elements with an elastic material model, the constraint of the superstructure on the cap beam disappeared and the residual lateral deflection at the top increased rapidly by comparing the detailed FE model with simplified FE Models VI and VII. In addition, simplified FE Model VI leads to higher second peak impact force and larger residual lateral deflection at the midheight than the detailed FE model. Although simplified FE Model VII has similar residual lateral deflection at the top with the detailed FE model, the second peak impact force predicted by the former is lower than that predicted by the latter. It shows that simplifying the superstructure into a rigid mass body does not accurately predict the dynamic responses of the CFST pier subject to truck impact.

Fig. 11 also shows the plastic strain and damage distribution of the detailed and simplified FE models. It should be noted that for the concrete material, the effective plastic strain output from LS-DYNA (LSTC 2020) is a damage level index which is a function of plastic strain. The concrete material is in the state of hardening when the damage level index ranges from 0 to 1, while it is in the state of softening when the damage level index ranges from 1 to 2. It can be seen that all the simplified FE models cannot present similar plastic strain and damage distribution of the CFST pier, the steel tube, and/or the core concrete with the detailed FE model. Therefore, the simplified FE models cannot completely replace the detailed FE model to simulate the performance of CFST piers subject to a truck collision. The detailed FE model is confirmed to be used for further performance evaluation.

Performance Evaluation of CFST Piers under Vehicle Collision

Based on the detailed FE model developed previously, the vehicular collision performances of CFST piers designed previously according to current codes in the US (AASHTO 2020; AISC 2010), Europe (CEN 2005a, b), and China (MOT 2015; MOHURD 2014) were evaluated herein.

Database for the Evaluation

Table 4 shows that the twelve CFST piers designed previously have considered the following effect factors: current codes in the three countries or regions, whether or not the vehicular collision load is considered, and two pier heights. In order to evaluate the performance of CFST piers under vehicle collision comprehensively, the influences of 20- and 40-ton trucks at impact speeds of 60, 100, and 140 km/h were also taken into account. Thus, a total of 72 numerical simulations were conducted based on the detailed FE model, as listed in Table 4.

Performance Levels of CFST Piers under Truck Collision

Numerical results show that CFST piers after the truck collision are classified into four damage states according to the characteristic of plastic strain and damage distribution and the extent of lateral deformation of CFST piers, as depicted in Fig. 12. The four damage states are described as follows:

1. Insignificant damage—No plastic strain occurs in the steel tube, and damage to core concrete mostly happens at the impact position of the CFST pier, and no lateral deflection takes place at the top of the CFST pier, as shown in Fig. 12(a).
2. Slight damage—Plastic strain of the steel tube and damage of core concrete primarily happen at the impact position and the foot of the CFST pier, and a slight lateral deflection occurs at the top of the CFST pier, as shown in Fig. 12(b).
3. Moderate damage—Plastic strain of the steel tube and damage of core concrete mostly takes place in the region from the midheight to the foot of the CFST pier, and a small lateral deflection happens at the top of the CFST pier, as shown in Fig. 12(c).
4. Severe damage—Plastic strain of the steel tube occurs in the region from the midheight to the foot of the CFST pier, and damage to core concrete happens almost throughout the CFTP pier, and a large lateral deflection takes place at the top of the CFST pier, as shown in Fig. 12(d).

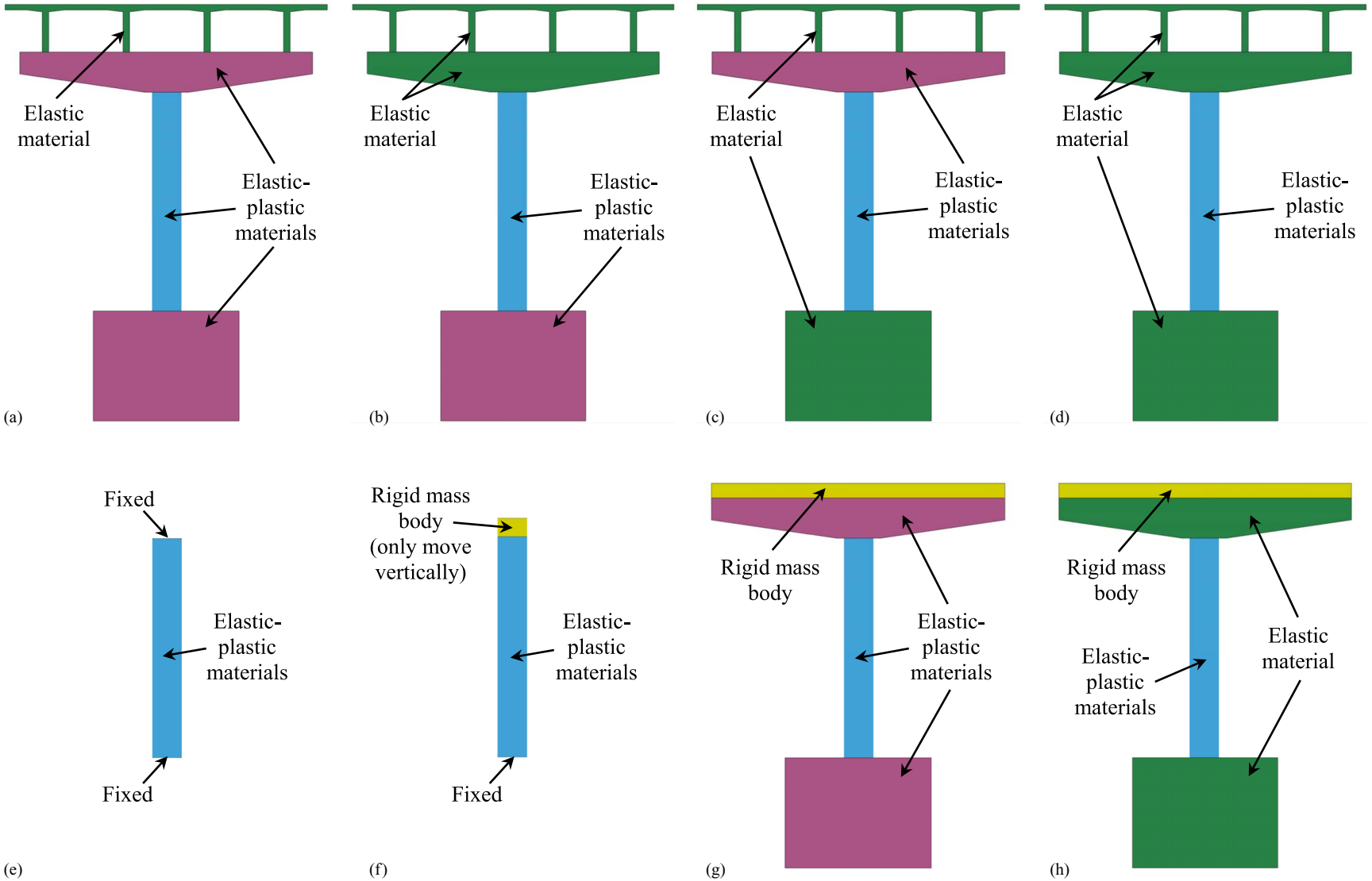

Fig. 9. Detailed and simplified FE models: (a) detailed FE model; (b) simplified FE Model I; (c) simplified FE Model II; (d) simplified FE Model IIII; (e) simplified FE Model IV; (f) simplified FE Model V; (g) simplified FE Model VI; and (h) simplified FE Model VII.

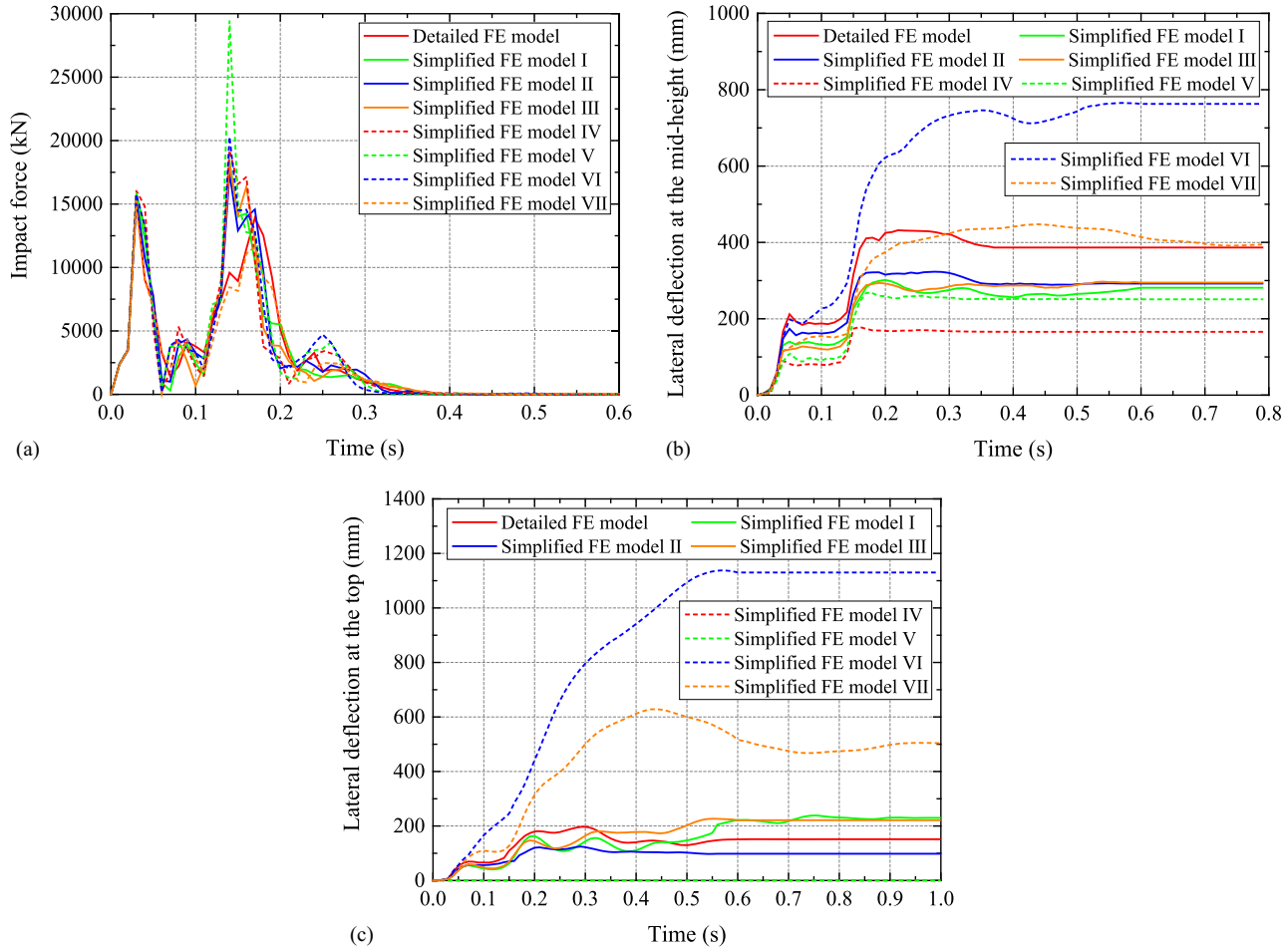

Fig. 10. Comparisons between detailed and simplified FE models: (a) impact force versus time curves; (b) lateral deflection at the midheight versus time curves; and (c) lateral deflection at the top versus time curves.

Based on the four damage states observed previously, four corresponding performance levels are defined for CFST piers under truck collision, which are listed in Table 8 and presented as follows:

1. Operational (OP)—The CFST pier is nearly undamaged under truck collision, and the operation of the bridge can be continued without any treatment for the CFST pier.
2. Immediate occupation (IO)—The CFST pier suffers slight damage under truck collision, and the bridge can be operated immediately after a minor repair of the CFST pier.
3. Life safety (LS)—The CFST pier underdoes moderate damage under truck collision, and the operation of the bridge should be closed instantly for a major repair of the CFST pier.
4. Collapse prevention (CP)—The CFST pier experiences severe damage, but the bridge does not collapse under truck collision, and the operation of the bridge must be closed instantly for partial or full replacement of the CSFT pier.

Evaluation Results and Discussion

According to the definitions of four damage states and four performance levels, the performance levels of CFST piers subjected to truck collision in all numerical simulations were determined, as listed in Table 4. Fig. 13 also shows the comparisons of the vehicular collision performance levels of CFST piers designed according to current codes in the US, Europe, and China.

It can be seen from Table 4 and Fig. 13 that only one CFST pier under vehicle collision, i.e., the 600 × 12 × 6 m CFST pier under the 40-ton and 140-km/h truck collision, presents the performance level of CP. However, the damage to the CFST pier does not result in the collapse of the bridge structure, as shown in Fig. 12(d). It means that the CFST piers designed according to current codes in the US (AASHTO 2020; AISC 2010), Europe (CEN 2005a, b), and China (MOT 2015; MOHURD 2014) are relatively safe under truck collision regardless of whether the vehicle collision load is considered.

When the vehicular collision load is ignored in the design, the performance levels of CFST piers designed according to current codes in the US (AASHTO 2020; AISC 2010) are not worse than those designed according to current codes in Europe (CEN 2005a, b) and China (MOT 2015; MOHURD 2014). When the vehicular collision load is considered, the performance levels of several CFST piers designed according to current codes in Europe (CEN 2005a, b) are significantly improved, while the performance levels of all CFST piers designed according to current codes in the US (AASHTO 2020; AISC 2010) and China (MOT 2015; MOHURD 2014) are rarely improved. However, as listed in Table 1, BS EN 1992-2 (CEN 2005a), and JTG D60-2015 (MOT 2015) specify the same value, i.e., 1,000 kN, for the vehicular collision load, which is much lower than the value of 2,700 kN suggested by AASHTO LRFDBDS-9 (AASHTO 2020). It implies that considering the vehicular collision load does not necessarily enhance the performance of CFST piers. It is because the design of a CSFT pier is a systematic project, which needs to comprehensively consider design values and

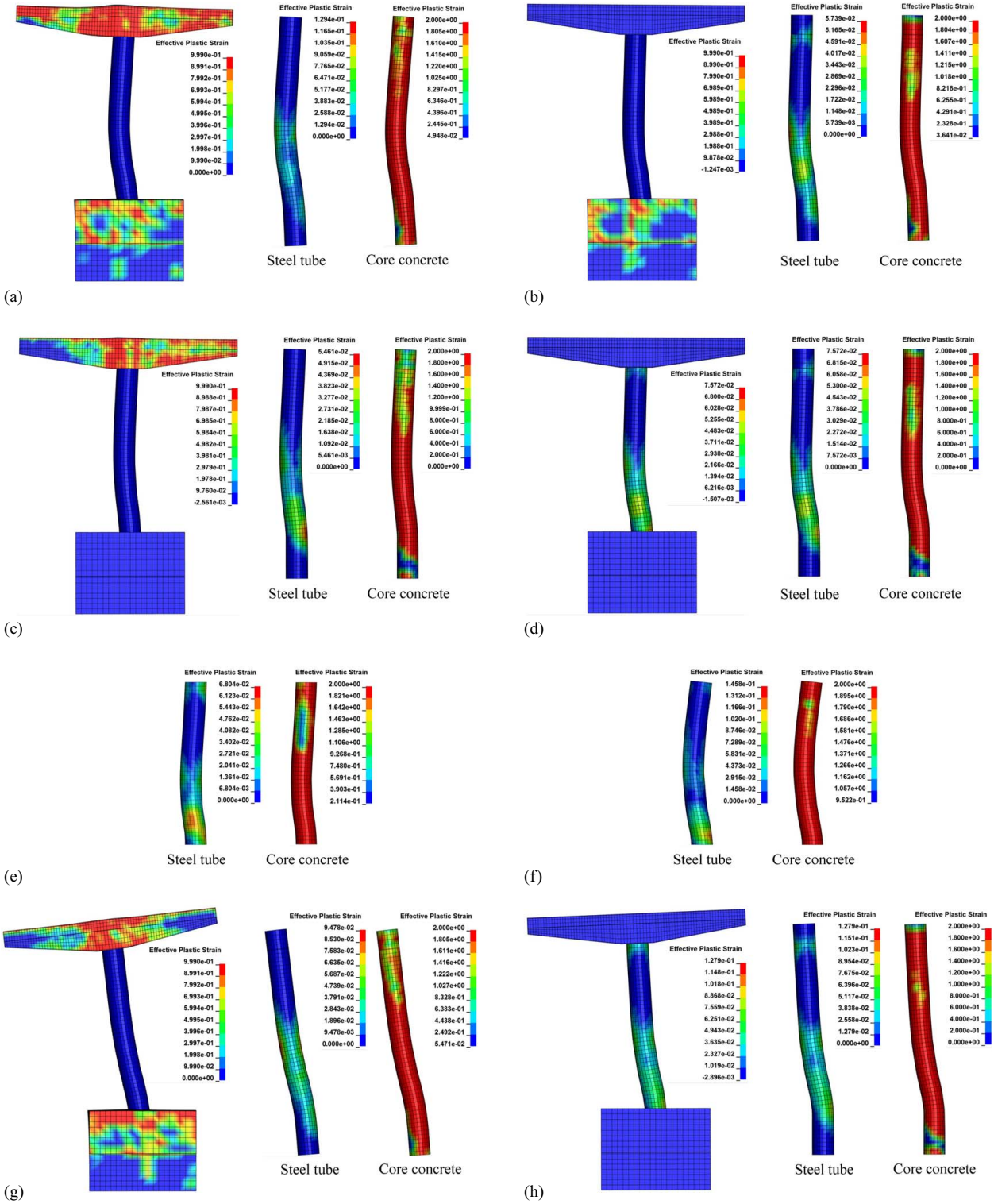

Fig. 11. Comparisons of plastic strain and damage distribution between detailed and simplified FE models: (a) detailed FE model; (b) simplified FE Model I; (c) simplified FE Model II; (d) simplified FE Model III; (e) simplified FE Model IV; (f) simplified FE Model V; (g) simplified FE Model VI; and (h) simplified FE Model VII.

combinations of multiple actions, bearing capacity check, and detailing requirements, as listed in Tables 1–3, respectively. The vehicular collision load is only one of the accidental actions. Therefore, in order to improve the performance of a CFST pier under vehicle collision, it is not enough to unilaterally increase the design value of the vehicular collision load, but it is also necessary to combine other design provisions of the current bridge and structural codes. For current codes in the US (AASHTO 2020; AISC 2010) and China (MOT 2015; MOHURD 2014), the design values of the vehicular collision loads have little effect on the performance of CFST piers. Hence, it is recommended that when a CFST pier in seismic zones is designed to resist vehicle collision in accordance with current codes in the US (AASHTO 2020; AISC 2010) and China (MOT 2015; MOHURD 2014), it

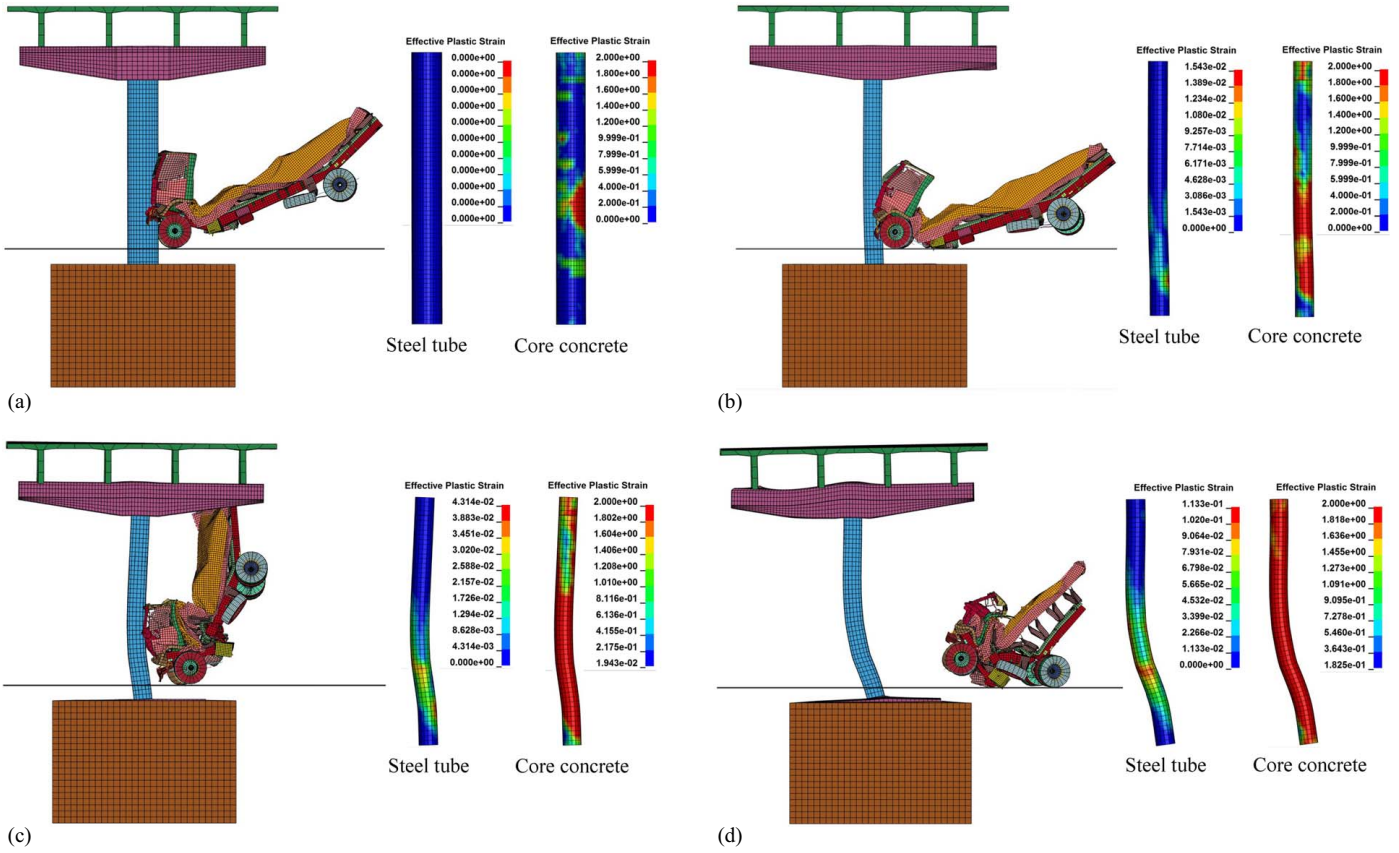

Fig. 12. Damage states of CFST piers after truck collision: (a) insignificant damage (e.g., 1,000 × 17 × 6 m, 40 tons, 60 km/h); (b) slight damage (e.g., 600 × 12 × 6 m, 40 tons, 60 km/h); (c) moderate damage (e.g., 600 × 12 × 6 m, 40 tons, 100 km/h); and (d) severe damage (e.g., 600 × 12 × 6 m, 40 tons, 140 km/h).

Table 8. Performance levels of CFST piers subjected to truck collision

Performance level	Damage state	Descriptions of performance level	
		CFST pier	Bridge
OP	Insignificant damage	No treatment	Can continue to be operated
IO	Slight damage	Minor repair	Can be operated immediately after repair
LS	Moderate damage	Major repair	Should be closed instantly for repair
CP	Severe damage	Replacement	Does not collapse but must be closed instantly for replacement

only needs to meet the requirements of seismic design without additional consideration of the vehicular collision load.

When the truck weight increases from 20 to 40 tons and/or the impact speed increases from 60 to 140 km/h, the performance of CFST piers degrades. It is attributed to the increase in collision kinetic energy. More collision kinetic energy leads to more serious damage to CFST piers. However, when the pier height increases from 6 to 12 m, the effect of the truck weight on the performance of CFST piers becomes small, especially no effect on the performance of CFST piers designed according to current codes in the US (AASHTO 2020; AISC 2010). This is because CFST piers designed in accordance with current codes in the US (AASHTO 2020; AISC 2010) have larger sectional dimensions, as listed in Table 4, resulting in larger sectional stiffness. Then, under the same collision, the deformation, damage, and energy dissipation of the CFST piers decrease, while those of the trucks increase. Because the extent of the deformation and damage of the CFST piers is small, the change in the performance levels is not significant with the increase in the truck weight. It demonstrates that CFST piers designed according to current codes in the US (AASHTO 2020; AISC 2010) are more conservative.

Interestingly, when the truck weight is 20 tons and the pier height is 12 m, CFST piers designed according to current codes in the US (AASHTO 2020; AISC 2010), Europe (CEN 2005a, b), and China (MOT 2015; MOHURD 2014) have the same performance levels at the same impact speeds regardless of whether the vehicular collision load is considered. When the truck weight increases from 20 tons to 40 tons and/or the pier height decreases from 12 m to 6 m, CFST piers designed according to current codes in the US (AASHTO 2020; AISC 2010), Europe (CEN 2005a, b), and China (MOT 2015; MOHURD 2014) present worse performance. Among them, the performance of CFST piers designed according to current codes in Europe (CEN 2005a, b) is significantly affected by whether or not the vehicular collision is considered. It seems that a shorter CFST pier under the collision of a heavier truck suffers more serious damage. For CFST piers designed according to current codes in Europe (CEN 2005a, b), the vehicular collision load does not need to be considered under any condition. A preliminary application condition should be added for the vehicular collision load specified by the current bridge code in Europe (CEN 2005a), that is, when the truck weight is more than 20 tons and/or the pier height is lower than 12 m.

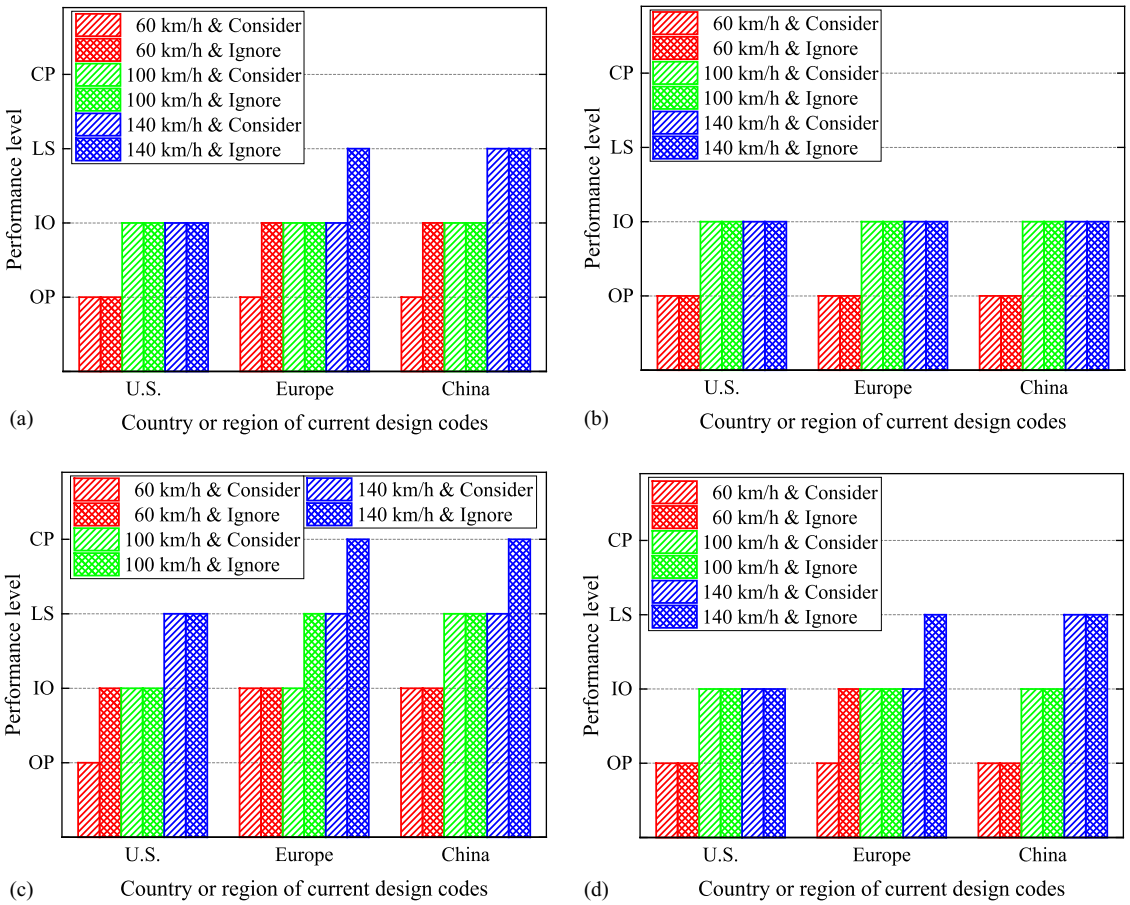

Fig. 13. Comparisons of performance levels of CFST piers: (a) truck weight of 20 tons and pier height of 6 m; (b) truck weight of 20 tons and pier height of 12 m; (c) truck weight of 40 tons and pier height of 6 m; and (d) truck weight of 40 tons and pier height of 12 m. *Consider* and *Ignore* refer to that the vehicle collision load is considered and ignored, respectively, during the design of the CFST pier.

Conclusions

This paper presents a vehicular collision performance evaluation of CFST piers designed in accordance with current bridge and structural codes in the US, Europe, and China. Before the evaluation, a detailed FE model for simulating vehicle collision with a CFST pier is developed, validated, and confirmed. The main conclusions are as follows:

1. The simplification of boundary components does not achieve the accuracy of the detailed FE model. Hence, a detailed FE model, where the superstructure is modeled using the elastic material model and the cap beam and substructure are modeled using the elastic–plastic material models, is suggested to be used to simulate the behavior of CFST piers under vehicle collision.
2. CFST piers designed according to current codes in the three countries or regions are relatively safe under truck collision regardless of whether the vehicle collision load is considered. Among them, CFST piers designed in accordance with current codes in the US (AASHTO 2020; AISC 2010) are more conservative.
3. When a CFST pier in seismic zones is designed to resist vehicle collision in accordance with current codes in the US (AASHTO 2020; AISC 2010) and China (MOT 2015; MOHURD 2014), it only needs to meet the requirements of seismic design without additional consideration of the vehicular collision load.
4. A preliminary application condition should be added for the vehicular collision load specified by the current bridge code in Europe (CEN 2005a), that is, when the truck weight is more than 20 tons and/or the pier height is lower than 12 m.

This study focuses on the influence of the vehicular collision load on the performance of CFST piers designed according to current codes in the three countries or regions. There are other factors that may affect the behavior of CFST piers under vehicle impact, including collision energy absorption measures and bearing types. Further work should study the effects of these factors.

Data Availability Statement

All data used during the study appear in the published article.

Acknowledgments

The financial support for this work from the National Natural Science Foundation of China under Grant No. 51408175 is greatly appreciated.

References

AASHTO. 2020. *LRFD bridge design specifications*. 9th ed. AASHTO LRFDBDS-9. Washington, DC: AASHTO.

Abdelkarim, O. I., and M. A. ElGawady. 2017. "Performance of bridge piers under vehicle collision." *Eng. Struct.* 140: 337–352. https://doi.org/10.1016/j.engstruct.2017.02.054.

AISC. 2010. *Specification for structural steel buildings*. ANSI/AISC 360-10. Chicago: AISC.

Auyeung, S., A. Alipour, and D. Saini. 2019. "Performance-based design of bridge piers under vehicle collision." *Eng. Struct.* 191: 752–765. https://doi.org/10.1016/j.engstruct.2019.03.005.

Buth, C. E., W. F. Williams, M. S. Brackin, D. Lord, S. R. Geedipally, and A. Y. Abu-Odeh. 2010. *Analysis of large truck collisions with bridge piers: Phase 1. Report of guidelines for designing bridge piers and abutments for vehicle collisions*. Rep. No. FHWA/TX-10/9-4973-1. College Station, TX: Texas Transportation Institute.

Cao, R., A. K. Agrawal, S. El-Tawil, X. Xu, and W. Wong. 2019a. "Heavy truck collision with bridge piers: Computational simulation study." *J. Bridge Eng.* 24 (6): 04019052. https://doi.org/10.1061/(ASCE)BE.1943-5592.0001398.

Cao, R., A. K. Agrawal, S. El-Tawil, X. Xu, and W. Wong. 2019b. "Performance-based design framework for bridge piers subjected to truck collision." *J. Bridge Eng.* 24 (7): 04019064. https://doi.org/10.1061/(ASCE)BE.1943-5592.0001423.

Cao, R., S. El-Tawil, A. K. Agrawal, X. Xu, and W. Wong. 2019c. "Behavior and design of bridge piers subjected to heavy truck collision." *J. Bridge Eng.* 24 (7): 04019057. https://doi.org/10.1061/(ASCE)BE.1943-5592.0001414.

CEN (European Committee for Standardization). 2005a. *Design of concrete structures—Part 2: Concrete bridges—Design and detailing rules*. Eurocode 2. BS EN 1992-2. Brussels, Belgium: CEN.

CEN (European Committee for Standardization). 2005b. *Design of composite steel and concrete structures—Part 2: General rules and rules for bridges*. Eurocode 4. BS EN 1994-2. Brussels, Belgium: CEN.

Chen, L., S. El-Tawil, and Y. Xiao. 2017. "Response spectrum-based method for calculating the reaction force of piers subjected to truck collisions." *Eng. Struct.* 150: 852–863. https://doi.org/10.1016/j.engstruct.2017.07.092.

Chen, L., J. Qian, B. Tu, D. M. Frangopol, and Y. Dong. 2021. "Performance-based risk assessment of reinforced concrete bridge piers subjected to vehicle collision." *Eng. Struct.* 229: 111640. https://doi.org/10.1016/j.engstruct.2020.111640.

Chen, L., H. Wu, and T. Liu. 2020. "Shear performance evaluation of reinforced concrete piers subjected to vehicle collision." *J. Struct. Eng.* 146 (4): 04020026. https://doi.org/10.1061/(ASCE)ST.1943-541X.0002571.

Do, T. V., T. M. Pham, and H. Hao. 2018. "Dynamic responses and failure modes of bridge columns under vehicle collision." *Eng. Struct.* 156: 243–259. https://doi.org/10.1016/j.engstruct.2017.11.053.

Do, T. V., T. M. Pham, and H. Hao. 2019. "Impact force profile and failure classification of reinforced concrete bridge columns against vehicle impact." *Eng. Struct.* 183: 443–458. https://doi.org/10.1016/j.engstruct.2019.01.040.

El-Tawil, S., E. Severino, and P. Fonseca. 2005. "Vehicle collision with bridge piers." *J. Bridge Eng.* 10 (3): 345–353. https://doi.org/10.1061/(ASCE)1084-0702(2005)10:3(345).

Fan, W., X. Xu, Z. Zhang, and X. Shao. 2018. "Performance and sensitivity analysis of UHPFRC-strengthened bridge columns subjected to vehicle collisions." *Eng. Struct.* 173: 251–268. https://doi.org/10.1016/j.engstruct.2018.06.113.

fib (fédération internationale du bétons). 2013. *Model code for concrete structures 2010*. *fib* Model Code 2010. Lausanne, Switzerland: fib.

Han, L.-H., C.-C. Hou, X.-L. Zhao, and K. J. R. Rasmussen. 2014. "Behaviour of high-strength concrete filled steel tubes under transverse impact loading." *J. Constr. Steel Res.* 92: 25–39. https://doi.org/10.1016/j.jcsr.2013.09.003.

Heng, K., R. W. Li, Z. R. Li, and H. Wu. 2021. "Dynamic responses of highway bridge subjected to heavy truck impact." *Eng. Struct.* 232: 111828. https://doi.org/10.1016/j.engstruct.2020.111828.

Hosseini, P., S. H. Ghasemi, M. Jalayer, and A. S. Nowak. 2019. "Performance-based reliability analysis of bridge pier subjected to vehicular collision: Extremity and failure." *Eng. Fail. Anal.* 106: 104176. https://doi.org/10.1016/j.engfailanal.2019.104176.

Li, R. W., H. Wu, Q. T. Yang, and D. F. Wang. 2020. "Vehicular impact resistance of seismic designed RC bridge piers." *Eng. Struct.* 220: 111015. https://doi.org/10.1016/j.engstruct.2020.111015.

LSTC (Livermore Software Technology Corporation). 2020. *LS-DYNA R12 keyword user's manual*. Livermore, CA: LSTC.

MOC (Ministry of Construction of the People's Republic of China). 2006. *Construction of concrete filled steel tubular structures*. [In Chinese.] GJBT-919. Beijing: MOC.

MOHURD (Ministry of Housing and Urban-Rural Development of the People's Republic of China). 2014. *Technical code for concrete filled steel tubular structures*. [In Chinese.] GB 50936-2014. Beijing: MOHURD.

MOT (Ministry of Transport of the People's Republic of China). 2015. *General specifications for design of highway bridges and culverts*. [In Chinese.] JTG D60-2015. Beijing: MOT.

MOT (Ministry of Transport of the People's Republic of China). 2020. *Specifications for seismic design of highway bridges*. [In Chinese.] JTG/T 2231-01-2020. Beijing: MOT.

NCAC (FHWA/NHTSA National Crash Analysis Center). 2011. "Finite element model archive." Accessed December 1, 2012. http://www.ncac.gwu.edu/vml/models.html.

Saini, D., and B. Shafei. 2019. "Performance of concrete-filled steel tube bridge columns subjected to vehicle collision." *J. Bridge Eng.* 24 (8): 04019074. https://doi.org/10.1061/(ASCE)BE.1943-5592.0001439.

Sharma, H., P. Gardoni, and S. Hurlebaus. 2015. "Performance-based probabilistic capacity models and fragility estimates for RC columns subject to vehicle collision." *Comput.-Aided Civ. Infrastruct. Eng.* 30: 555–569. https://doi.org/10.1111/mice.12135.

Sharma, H., S. Hurlebaus, and P. Gardoni. 2012. "Performance-based response evaluation of reinforced concrete columns subject to vehicle impact." *Int. J. Impact Eng.* 43: 52–62. https://doi.org/10.1016/j.ijimpeng.2011.11.007.

Stephens, M. T., D. E. Lehman, and C. W. Roeder. 2016. "Design of CFST column-to-foundation/cap beam connections for moderate and high seismic regions." *Eng. Struct.* 122: 323–337. https://doi.org/10.1016/j.engstruct.2016.05.023.

Wang, R., L.-H. Han, and C.-C. Hou. 2013. "Behavior of concrete filled steel tubular (CFST) members under lateral impact: Experiment and FEA model." *J. Constr. Steel Res.* 80: 188–201. https://doi.org/10.1016/j.jcsr.2012.09.003.

Wu, M., L. Jin, and X. Du. 2020. "Dynamic responses and reliability analysis of bridge double-column under vehicle collision." *Eng. Struct.* 221: 111035. https://doi.org/10.1016/j.engstruct.2020.111035.